AD-A273 307

REPORT DOCUMENTATION PAGE

Form Approved
OMB No 0704-0188

2

...average 1 hour per response, including the time for reviewing instructions, searching existing data sources ... the collection of information. Send comments regarding this burden estimate or any other aspect of this ... to Washington Headquarters Services, Directorate for Information Operations and Reports, 1215 Jefferson ... Management and Budget, Paperwork Reduction Project (0704-0188), Washington, DC 20503

1. AGENCY USE ONLY (Leave blank)	2. REPORT DATE	3. REPORT TYPE AND DATES COVERED
	23 Nov., 1993	Technical 8/1/92 - 7/31/93

4. TITLE AND SUBTITLE

"The Nanometer-Scale Mechanics of Gold Films"

5. FUNDING NUMBERS

N00014-91-J-1991

6. AUTHOR(S)

P. Tangyunyong; R. C. Thomas; J. E. Houston; T. A. Michalske; R. M. Crooks; A. J. Howard

7. PERFORMING ORGANIZATION NAME(S) AND ADDRESS(ES)

Department of Chemistry
University of New Mexico
Albuquerque, NM 87131

8. PERFORMING ORGANIZATION REPORT NUMBER

7

9. SPONSORING/MONITORING AGENCY NAME(S) AND ADDRESS(ES)

Office of Naval Research
800 North Quincy Street
Arlington, VA 22217-5000

10. SPONSORING/MONITORING AGENCY REPORT NUMBER

11. SUPPLEMENTARY NOTES

Prepared for publication in *Phys. Rev. Lett.*

12a. DISTRIBUTION/AVAILABILITY STATEMENT

This document has been approved for public release and sale; its distribution is unlimited.

12b. DISTRIBUTION CODE

N00179

13. ABSTRACT (Maximum 200 words)

We have used interfacial force microscopy (IFM) to monitor the mechanical deformation of single nanometer-sized grains in Au thin films. Our results show that protruding grains, which represent early-stage delamination, display multiple deformation mechanisms including grain-boundary sliding and intra-granular plasticity. The unprecedented load displacement control capability of the IFM provides data that is used for the first time to quantitatively distinguish and evaluate individual deformation processes.

14. SUBJECT TERMS	15. NUMBER OF PAGES
	14
	16. PRICE CODE

17. SECURITY CLASSIFICATION OF REPORT	18. SECURITY CLASSIFICATION OF THIS PAGE	19. SECURITY CLASSIFICATION OF ABSTRACT	20. LIMITATION OF ABSTRACT
Unclassified	Unclassified	Unclassified	

OFFICE OF NAVAL RESEARCH

GRANT N00014-91-J-1991

R&T Code s400x084yip01

Technical Report No. 7

The Nanometer-Scale Mechanics of Gold Films

by

P. Tangyunyong, R. C. Thomas, J. E. Houston,
T. A. Michalske, R. M Crooks, and A. J. Howard

Prepared for Publication
in
Phys. Rev. Lett.

Department of Chemistry
University of New Mexico
Albuquerque, NM 87131
November 23, 1993

6-30-93

The Nanometer-Scale Mechanics of Gold Films

P. Tangyunyong,* R. C. Thomas,† J. E. Houston,*
T. A. Michalske,* R. M. Crooks,† and A. J. Howard*

*Sandia National Laboratories, Albuquerque, New Mexico
†Department of Chemistry, University of New Mexico,
Albuquerque, New Mexico

We have used interfacial force microscopy (IFM) to monitor the mechanical deformation of single nanometer-size grains in Au thin films. Our results show that protruding grains, which represent early-stage delamination, display multiple deformation mechanisms including grain-boundary sliding and intra-granular plasticity. The unprecedented load-displacement control capability of the IFM provides data that is used for the first time to quantitatively distinguish and evaluate individual deformation processes.

PACS #: 62.20.Dc; 62.20.Fe

7.

Nano-structured materials have recently received considerable attention because of their potential for enhanced mechanical properties such as supermodulus[1] or superplastic behavior[2]. The mechanical properties of these materials depend on a complex interplay between the nano-grains, and one of the limiting factors in their development involves the difficulty of performing mechanical measurements at this size level. In this paper, we present results of the application of interfacial-force microscopy (IFM)[3-5] to the first quantitative determination of the deformation properties for single, nm-size grains in polycrystalline Au thin films.

One of the oldest and most widely used techniques for local determinations of deformation properties involves surface indentation--measuring elastic moduli, plastic behavior, hardness, etc., by an analysis of the loading behavior of a small probe deforming a substrate surface (interfacial force vs. substrate deformation). Compared to the ultra-microindenter[6], the nanoindenter[7] and, more recently, the atomic force microscope[8], the IFM is characterized by its use of a self-balancing force sensor which permits both mechanically stable and quantitative load-displacement control.

In the present study, we combine the methods of contact mechanics and classic indentation techniques to quantitatively determine an individual grain's elastic constant and its shear-stress threshold for plastic deformation. Au films were chosen for this study because we previously found that Au surfaces could be passivated against probe-surface adhesion with a self-assembling *n*-alkanethiol monolayer film: passivation which was maintained even under large compressive stresses[5]. The adhesion

passivation permits a direct application of contact mechanics to quantitatively analyze the local deformation response.

Polycrystalline Au films 200 nm thick were prepared by thermal-vapor deposition onto 300 C clean-glass substrates at a rate of 0.2 nm/sec. The deposition was followed by a three-hour anneal at 275 C. The films were subsequently cleaned in a 3:1 concentrated H_2SO_4:30% H_2O_2 solution. Self-assembling monolayer films were adsorbed by soaking the Au films in 0.5 mM *n*-octadecanethiol/ethanol solutions for 36 hours. To insure uniform coverage, the monolayers were characterized by ellipsometry and Fourier transform infrared external reflectance spectroscopy.

The W probe was prepared by electrochemically etching a 0.1 mm wire in potassium hydroxide (KOH) solution. The probe was characterized by scanning electron microscopy (SEM) and found to have a parabolic shape with an apex radius of curvature of ~250 nm. All measurements were conducted in air with both sample and probe immersed in hexadecane to eliminate capillary interactions. Topological images were taken in the constant repulsive-force mode at a load level of 0.5 μN. IFM loading data (load vs. displacement) were obtained using a force-feedback, constant *deformation-rate* mode at a rate of 20 nm/sec.

IFM images show that the Au surface is dominated by large flat grains with a narrow distribution of grain sizes averaging ~500 nm in diameter. Occasionally, we also see grains which protrude above the nominally flat surface by 10 to 30 nm. Fig. 1(a) shows an example of an IFM image of such a protruding grain. We focus first on the mechanics of protruding grains because they show the full range of deformation response encountered on

these films, and then we summarize the results for a number of experiments on more typical grains.

We perform a loading-cycle experiment by first placing the probe over the center of the selected grain. The surface is then moved toward the probe at a constant rate. At a predetermined repulsive load, we withdraw the probe at the same rate. This produces a load-displacement curve where contact is defined as the point where the load begins to go repulsive. The loading-cycle curve for the grain of Fig. 1(a) is shown in Fig. 2(a). These data show a large hysteresis loop between loading and unloading, which indicates an irreversible deformation.

Detailed analysis reveals that there are three distinct regions in the loading portion of the cycle as indicated in Fig. 2(a). In the first region, we find no hysteresis for peak loads less than ~6 μN. In addition, the relationship between load and deformation closely follows the classical Hertzian model for a rigid, non-interacting parabolic punch deforming an elastic half space[9]. According to this model, the applied load scales as the three-halves power of the surface displacement,which results from the change in contact area with increasing load. A comparison of the loading curve in region 1 with the Hertzian model is shown as a solid line in Fig. 2(a). Thus, we are elastically deforming the surface in region 1.

The point at which the loading curve deviates from Hertzian marks the onset of plastic deformation (region 2), which occurs at a load of ~6 μN. Above ~27 μN (region 3), the hysteresis loop closes and the deformation is again elastic, as born out by the Hertzian fit shown as the solid line in region 4.

Starting at the maximum load in region 4, the unloading curve consists of two distinct Hertzian-like regions (4 and 5 in Fig. 2(a)), which appears to be separated at a load of ~6 μN. Region 5 has the same elastic properties as region 1. Quantitatively, the effective elastic moduli of regions 1 and 3, derived from Hertzian analysis, are found to be 28 and 66 GPa, respectively.

After the loading cycle of Fig. 2(a), a repulsive-force image (Fig. 1(b)) was taken to clarify the nature of the plastic deformation seen in Fig. 2(a). The image clearly shows that the grain has not been indented but rather has been displaced into the surface by the probe, which suggests the availability of sub-surface free volume. Line scans across the center of the images indicate a total grain displacement of ~8 nm.

Repeating the loading procedure of Fig. 2(a) to a higher peak load results in the load-displacement curve of Fig. 2(b), which shows a hysteresis loop and five distinct regions of deformation behavior. Regions 1 and 2 are identical to regions 4 and 5 of the initial loading cycle of Fig. 2(a). The onset of plastic deformation (region 3) occurs at a load of ~44 μN and, using the SEM-measured tip radius and the Hertzian contact radius at this load, the shear-stress threshold can be calculated to be 1.7 GPa based on continuum elasticity theory[10].

Since region 4 shows no indication of loop closure at the higher loads, we associate this deformation with an actual indentation of the grain itself. An image taken after the second loading cycle (Fig. 1(c)) corroborates this assessment and, from line scans, the depth is found to be ~5 nm. Thus, the unloading curve in region 4 can be modeled by Sneddon's analysis of surface stiffness[11] based on the assumption that the contact area remains constant, i.e., the probe is imbedded in a permanently deformed socket. The result of

this analysis is shown as a dashed line in Fig. 2(b). An effective elastic modulus of 60 GPa is derived from this analysis using a contact area calculated form the indentation seen in Fig. 1(c). Region 5 has a Hertzian-like appearance and is representative of the last stages of elastic relaxation as the probe is removed from the indentation.

On the basis of the loading-cycle data and the images shown in Fig.1, we can identify the individual contributions of inter-granular and intra-granular plastic deformation during the loading cycle of Fig. 2(a). A schematic model summarizing these contributions is shown in Fig. 3(a). In region 1, the grain is elastically deformed by the probe, slightly sagging under the applied load. According to this proposed model, region 1 represents a combination of elastic-contact deformation and elastic sagging of the grain, which is supported by its neighbors. The elastic sagging of the nano-grain closely corresponds to a diaphragm loaded by a probe whose contact area varies with load and which becomes appreciable with respect to the grain size. Since both types of elastic deformation are nonlinear with load, it is not altogether surprising that the behavior appears Hertzian[12].

As the load is increased above 6 μN (region 2), the grain slips at it's boundary allowing the grain to slide into the surface and reduce the sub-surface free volume. Concurrent with the inter-granular displacement, the sagging increases with increasing load and the grain is further elastically deformed . This process continues until the grain comes into contact with the glass substrate, which marks the beginning of region 3.

In region 3, we see only elastic deformation, and there is no further grain-boundary sliding. The elastic behavior here is quite different from region 1, as evidenced by the large increase in measured elastic modulus

(from 28 GPa to 66 GPa). The smaller value represents the effect of the grain sagging as discussed above. In region 4, the grain recovers from the elastic strain of regions 2 and 3 while remaining in contact with the substrate. As the load is decreased further (region 5), the grain partially rebounds from the sagging imposed in regions 1 and 2. Subtracting the line-scan displacement (~8 nm) from the loading displacement (~12 nm) gives a total rebound of ~4 nm in region 5. Our conclusion concerning this behavior is supported by the fact that the effective elastic constant from the Hertzian analysis in region 5 is the same as that determined in region 1.

Similarly, we can identify the deformation modes in the second loading cycle of Fig. 2(b) from loading-cycle data and images, as summarized schematically in Fig. 3(b). As in Fig. 2(a), the grain is deformed elastically in region 1, slightly sagging into remaining free volume, until contact is again made with the substrate (beginning of region 2). In region 2, we only see elastic deformation. As expected, the elastic behavior of these two regions is the same as regions 4 and 5 during the first loading cycle. Higher loading results in the creation of a ~5 nm indention (region 3). A line-scan comparison indicates that there is an additional grain slippage prior to the indentation.

In region 4, the probe is embedded in a permanently deformed indentation and the contact area initially remains constant as the probe is removed. In region 5, we observe an elastic behavior which results from the final stages of probe removal from the indentation. We suggest that this region is the same as that observed in regions 1 and 2 as measured by a probe being removed from a socket, i.e., where the contact area is changing with load[13].

The elastic modulus found in this sample when the grain is in contact with the substrate (66 GPa) is about 20% smaller than the reference value of 78 GPa tabulated for bulk Au[14] and our measurement of 70 GPa for the same probe acting on a single-crystal Au(111) surface. This difference is not entirely surprising, since we are dealing here with supported Au thin films. In addition, we find from recent measurements that the elastic properties of the films vary strongly as a function of the substrate. For example, the effective elastic modulus of similar Au films on silicon substrates with chromium adhesion layers is about twice as large as those found in the present measurements (110 vs. 66 GPa) and the shear-stress threshold for plastic deformation reflects a similar difference (4.5 vs. 2.6 GPa)[5]. In addition, we find in a general survey of non-protruding grains that the loading-cycle data do not show the multi-region behavior found for the protruding grains (Fig. 2(a) and (b)). The values determined from this survey are 75 ±15 GPa and 2.7 ±0.5 GPa for the elastic modulus and the shear-stress threshold for plastic deformation, respectively.

The existence of protruding grains with free volume beneath is a sign of early-stage delamination. Au films do not adhere well to glass substrates and peel if immersed in the H_2SO_4:30% H_2O_2 cleaning solution for extended periods. It is likely that our brief surface cleaning procedure triggers the early stages of this delamination.

The quantitative values for the elastic modulus and shear-stress threshold for plastic deformation obtained here are, of course, not representative of bulk Au itself. Rather, these data take into account the various factors that characterize thin-film mechanical behavior, e.g., grain-boundary slippage and dimensionality effects imposed by interactions with a

substrate having differing mechanical properties. However, this kind of information is invaluable if we expect to be able to tailor the mechanical properties of nanophase materials.

This work is supported by the Office of Basic Energy Sciences, Division of Material Sciences, U.S. Department of Energy under Contract No. DE-AC04-76DP00789. R.C.T acknowledges the support of Associated Western Universities. R.M.C is supported by the Office of Naval Research.

Figure Captions

Fig. 1 400x400 nm IFM repulsive-force images of a typical protruding grain (a) before loading, (b) after a loading cycle to a peak load of ~35 μN, and (c) after a second loading cycle to a peak load of ~75 μN.

Fig. 2 (a) Load-cycle data taken in the center of the protruding grain shown in Fig. 1a to a peak load of ~35 μN. Solid lines represent the fits based on a Hertzian elastic analysis for a parabolic punch deforming an elastic half space[8]; (b) Loading-cycle taken at the same position to a peak load of ~75 μN. The dashed curve represents an analysis of the unloading curve based on Sneddon's model of a parabolic punch embedded in an indentation, i.e., constant contact area[11].

Fig. 3 Schematic model of the behavior of the protruding grain shown in Fig. 1(a). Arrows indicate the direction of motion of the probe and in (a) the numbers refer to the different regions shown in Fig. 2(a) while (b) refers to the regions in Fig. 2(b).

References

1. R. C. Cammarata, Scripta Metall. 20, 479 (1986).
2. *Superplasticity in Metals, Ceramics and Intermetallics*, Eds. M. J. Mayo, M. Kobayashi and J. Wadsworth, Mat. Res. Soc. Proc, Vol. 196, 1990.
3. S. A. Joyce and J. E. Houston, Rev. Sci. Instru. 62, 710 (1991).
4. J. E. Houston and T. A. Michalske, Nature 356, 266 (1992).
5. R. C. Thomas, J. E. Houston, T. A. Michalske, and R. M. Crooks, Science 259, 1883 (1993).
6. T. J. Bell, A. Bendeli, J. S. Field, M. V. Swain, and E. G. Thwaite, Metrologia 28, 463 (1991).
7. M. F. Doerner and W. D. Nix, J. Mater. Res. 1, 601 (1986).
8. M. Salmeron, A. Folch, G. Neubauer, M. Tomitori, D. F. Ogletree, and W. Kolbe, Langmuir 8, 2832 (1992).
9. I. N. Sneddon, Int. J. Eng. Sci. 3, 47 (1965).
10. S. P. Timoshenko and J. N. Goodier, Theory of Elasticity, (McGraw-Hill, New York, 1970).
11. G. M. Pharr, W. C. Oliver and F. R Brotzen, J. Mater. Res. 7, 613 (1992).
12. A. Blake, **Handbook of Mechanics, Materials and Structures** (John Wiley & Sons, New York,1985), p. 615.
13. J. S. Field and M. V. Swain, J. Mater. Res. 8, 297 (1993).
14. R. W. Hertzberg, **Deformation and Fracture Mechanics of Engineering Materials** (John Wiley & Sons, New York, 1976), Chap. 1.

Fig. 1

(a) (b) (c)

Fig. 2

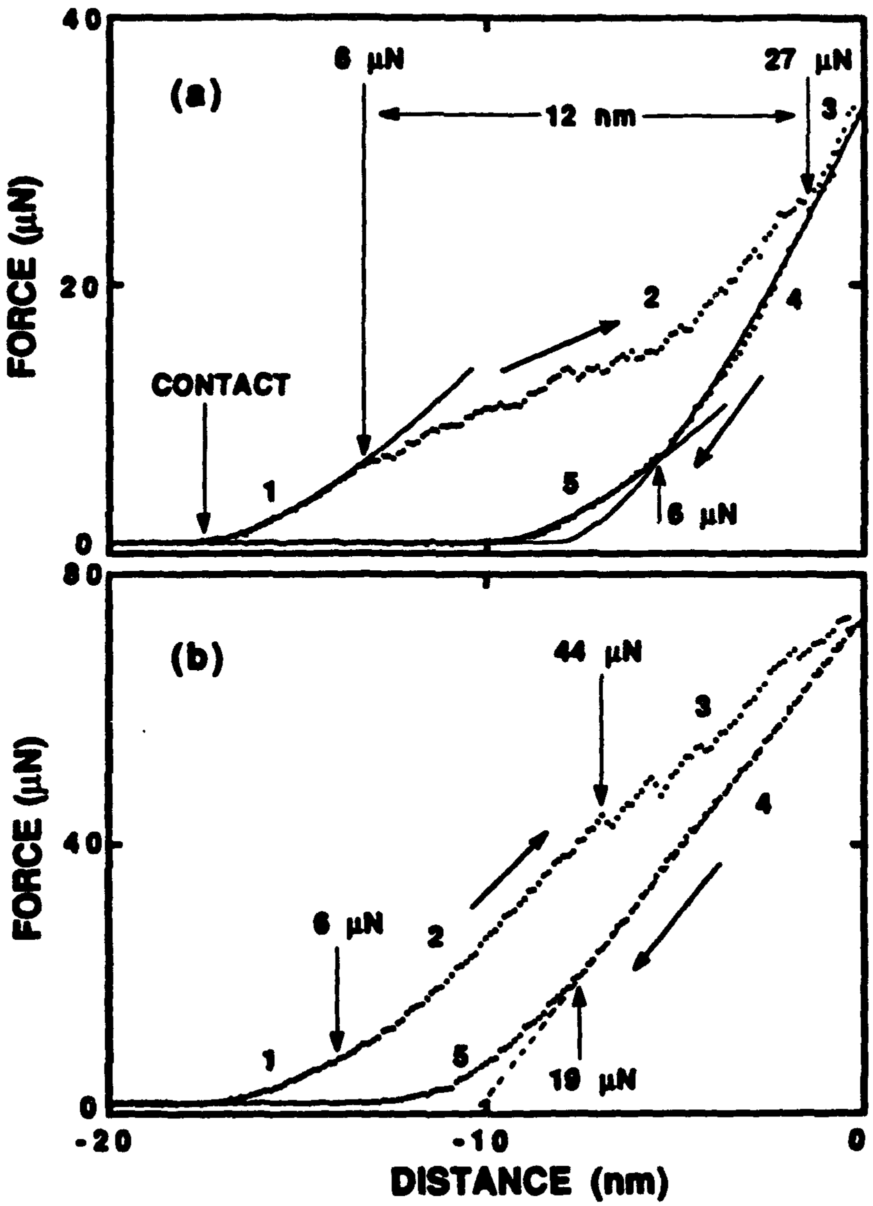

(a)
6 μN
27 μN
12 nm
3
2
4
CONTACT
1
5
6 μN
FORCE (μN)
40
20
0
(b)
44 μN
3
4
6 μN
2
1
5
19 μN
FORCE (μN)
80
40
0
-20
-10
0
DISTANCE (nm)

Fig. 3